Decentralized Power Management in a Hybrid Fuel Cell Ultracapacitor System

Omid Madani, Amit Bhattacharjee, and Tuhin Das, *Member, IEEE*

***Abstract*—This paper addresses decentralized control of a hybrid energy system consisting of a fuel cell (FC) and an ultracapacitor. Separate controllers are developed for the FC and the ultracapacitor for power management rather than one central controller. Explicit communication between controllers, such as exchange of locally sensed information, is absent. The former operates the FC in a load-following mode, while attenuating transient fluctuations in fuel utilization. The latter allows the ultracapacitor to be used as an energy buffer. The paper proposes a simple energy-conservation-based approach where the FC controller estimates the energy gap that is compensated for by the capacitor, based on its own transient response history. Accordingly, it modulates its own output power. The capacitor control, in turn, imparts robustness to the collective performance of the controllers by either dissipating excess energy or regulating the load voltage. Together, synergistic power management is achieved within a decentralized framework. An experimental test stand is developed to validate the approach and experimental results are provided. This paper considers one power source and one energy storage element, and further research must be done to translate this approach to power networks.**

***Index Terms*—Capacitor, decentralized control, energy storage, fuel cell (FC), hardware-in-the-loop, power management, stability.**

NOMENCLATURE

A	Area enclosed by power versus time profiles (J).
C	Capacitance of ultracapacitor (F).
C_1, C_2	Represents dc/dc converters.
E_A	Net change in capacitor energy (J).
F	Faraday's constant (= 96485.34 C/mol).
i	Current draw (A) (the relevant subscripts of i are L, fc, uc, and o).
k	Constant anode recirculation fraction.
K_1, K_2	Represents the two decentralized controllers.
$\dot{N}_{\text{air}}$	Molar flow rate of air (mols/s).
$\dot{N}_f$	Molar flow rate of fuel (mols/s).
$\dot{N}_{\text{in}}$	Anode inlet flow rate (mols/s).
$\dot{N}_o$	Anode exit flow rate (mols/s).
n	Number of electrons participating in electrochemical reaction (= 2).
$\mathcal{N}_{\text{cell}}$	Number of solid oxide fuel cells (SOFCs) in series (chosen as 50).
P	Power (W).
S_t	Target state of charge (SOC) of ultracapacitor.
U	Fuel utilization of SOFC.
V	Voltage (V) (Relevant subscripts: L, fc, and uc).
$\eta_1, \eta_2, \bar{\eta}_2$	Efficiencies of dc–dc converters.
μ	Duty ratio of pulsewidth modulation (PWM) circuit.
σ_R	Conductance of dissipating resistance (Ω^{-1}).
$\mathcal{X}$	Species mole fraction in gas mixture.
Subscripts	
a	Anode control volume.
cal	Calculated value.
d	Demand (relevant to $i_{\text{fc},d}$, $V_{\text{uc},d}$, and $\dot{N}_{f,d}$).
fc	Fuel cell (FC).
j, q	Indices of A representing deficient and excess power regions, respectively.
L	Load.
nom	Nominal.
o	Used to denote C_1's output-side current.
r	Reformate control volume.
ss	Steady State.
uc	Ultracapacitor.

Manuscript received September 9, 2014; revised April 30, 2015; accepted July 4, 2015. Date of publication August 27, 2015; date of current version April 18, 2016. Manuscript received in final form July 29, 2015. This work was supported by the National Science Foundation under Grant CMMI: 1158845. Recommended by Associate Editor S. Varigonda.

O. Madani and A. Bhattacharjee are with the University of Central Florida, Orlando, FL 32816 USA (e-mail: s.omid.madani@gmail.com; amit.bhattacharjee@knights.ucf.edu).

T. Das is with the Department of Mechanical and Aerospace Engineering, University of Central Florida, Orlando, FL 32816 USA (e-mail: tuhin.das@ucf.edu).

Color versions of one or more of the figures in this paper are available online at http://ieeexplore.ieee.org.

Digital Object Identifier 10.1109/TCST.2015.2464295

I. INTRODUCTION

SOFCs have drawn attention due to many benefits such as fuel flexibility, tolerance to impurities in fuels, high efficiency, and ability to use heat for cogeneration [1]–[3]. However, slow response time leading to deficient load-following capability is an obstacle that has restricted extensive application of SOFCs [4]. The issue is manifested as a susceptibility of SOFCs to hydrogen starvation when subjected to transient and fluctuating power demands (see details in [5] and the references therein).

In SOFCs, hydrogen starvation is mainly caused by the lags introduced by the fuel supply system (FSS) and the reformer [6]. To prevent this issue, [6] develops various reference governors using a model predictive approach. Mueller *et al.* [7] address this issue using a linear compensator to modify the target fuel flow. While both methods reduce the susceptibility to fuel starvation, they are both model dependent. Furthermore, both methods have an adverse effect

on the load-following capability of the SOFC. To improve load following, Mueller *et al.* [8] develop a control method based on constant utilization operation and a control structure to keep the combustor temperature within acceptable range. Hydrogen starvation in SOFCs can be prevented by limiting the fluctuations in fuel utilization from a set-point value under transient power demands. The target fuel utilization is typically chosen between 80% and 90% for high efficiency [9]–[11]. Prior work by one of the authors proposes a current regulation (CR) method to attenuate the aforementioned fluctuations in utilization. More details of this method and discussions on the importance of fuel utilization in SOFC systems can be found in [5], [12], [13], and the references therein. While works on transient control in SOFCs are limited in the literature, considerable research is reported for polymer electrolyte membrane (PEM) FCs under transient conditions, where oxygen starvation is a relevant problem [14]–[18].

Simultaneously preventing hydrogen starvation and improving load following can be achieved by hybridizing the SOFC with an energy storage device such as battery or capacitor [4], [5], [11], [13], [19]. For PEM FCs, related work in the area of hybridization has been addressed by Vahidi *et al.* [18] and Thounthong *et al.* [20]. In load-following mode, the storage acts as a buffer that supplies or absorbs energy during transients as the FC *follows* the changing load demand. Operating the FC in load-following mode rather than in base-load operation is advantageous since it reduces the required storage capacity. However, hybridization mandates the existence of a robust power management algorithm that ensures that the storage device is neither progressively depleted nor overcharged. Robust SOC preserving control strategies for SOFC ultracapacitor hybrids were proposed in [5] and [13]. These works demonstrate power management in the hybrid system via application of nonlinear and H_∞ robust control. A similar problem was identified in [11], where a control strategy that guarantees FC health and maintains system voltages around a nominal value was developed. A supervisory controller for a SOFC ultracapacitor hybrid, based on fuzzy logic, was designed in [21].

The works mentioned above can be categorized as *centralized* power management schemes where sensed information is directed toward a central processor that commands all components of the system. While centralized control is easier to develop, practical issues can arise in scaling up to bigger networks. When posed as an optimization problem, high dimensions is an issue for current microcontrollers as the number of energy resources in the network increases [22]. In addition, in case the central controller encounters any malfunction, the entire network is influenced. Furthermore, if the network topology is subject to change, a central controller may need to be reprogrammed. Hence, the idea of *decentralized* power management is worth exploring, where information processing takes place in component-level controllers that have little or no communication between each other, and a certain level of fault tolerance is built in. While the idea of decentralized control of SOFC appears in [23], it interprets decoupled proportional–integral–differential loops within the SOFC controller as decentralized control. In contrast, this paper considers decentralization in the context of power management in a network consisting of the SOFC and an ultracapacitor.

In recent years, there has been growing interest in distributed control in the context of large-scale networked systems. The size and the complexity of such systems necessitate decentralized control [24]–[26]. Decentralized control of power grids specifically appears in [27]–[31]. The SOFC is also deemed a fitting candidate for distributed generation in grids due to its many advantages [19], [32]–[34]. While addressing decentralized control in power networks is our ultimate goal, this paper formulates a simpler problem as a first step. We design decentralized control for a hybrid SOFC ultracapacitor system. Two separate controllers are proposed, one for the SOFC and the other for the ultracapacitor, which have no communication between each other. The former operates the FC in load-following mode, while attenuating transient fluctuations in the fuel utilization. The latter allows the ultracapacitor to be used as an energy buffer. The novelty of this paper lies in the energy-conservation-based mechanism that is incorporated in the SOFC controller. It anticipates the deficit or excess energy of the capacitor based on the SOFC's transient response history, without communicating with the ultracapacitor. The capacitor control, in turn, imparts robustness to the performance of the decentralized system by either dissipating excess energy or regulating the load voltage. Together, synergistic power management is realized.

In this paper, a description of the SOFC and a description of the hybrid system and a statement of the control objectives are given in Section II. The main principle of the proposed decentralized control is presented in Section III, along with practical designs of the two controllers that rely on controlled energy dissipation and provide robust performance. The work reported in this paper was verified using an experimental setup that was built by the authors. The setup is explained in Section IV. An alternate approach to incorporate robustness, based on load voltage modulation, is presented along with simulation and experimental data in Section V. A discussion on the energy loss trends of the two approaches and an advantage of decentralized over centralized control is presented in Section VI. Finally, the concluding remarks are stated and acknowledgments are made.

II. Background

A. SOFC System Description

The specific system considered in this paper is a steam-reformer-based SOFC system with methane as fuel, which is shown schematically in Fig. 1. The reformer produces a hydrogen-rich gas, which is supplied to the anode of the FC. Electrochemical reactions occurring at the anode due to current draw results in a steam-rich gas mixture at its exit. A known fraction k of the anode exhaust is recirculated through the reformer into a mixing chamber where fuel $\dot{N}_f$ is added. Fuel is supplied by the FSS. The FSS consists of a fuel pump and/or valves and a fuel flow controller. The heat required for

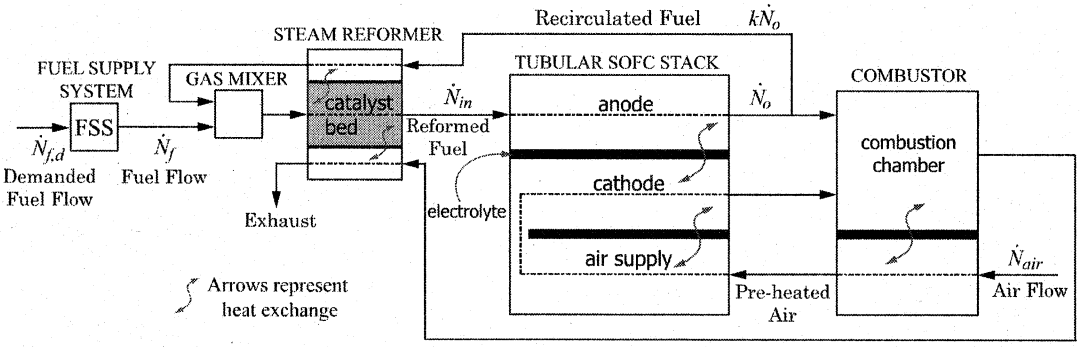

Fig. 1. Schematic of the SOFC system.

sustaining the endothermic steam reforming process occurring in the reformer catalyst bed is supplied from two sources, namely, the combustor exhaust that is passed through the reformer and the aforementioned recirculated anode flow. The combustor also serves to preheat the cathode air $\dot{N}_{\text{air}}$. The tubular construction of each cell causes the air to first enter the cell through the air supply tube and then reverse its direction to enter the cathode chamber. We use a control-oriented mathematical model of a tubular SOFC system developed and presented in [12] for control validation. The model captures the thermodynamics, chemical kinetics, heat transfer, and pressure dynamics phenomena and has been validated against the results in [35] and [36].

B. Current Regulation

A strategy for attenuating transient fluctuations in fuel utilization developed in [13] and [37] will be outlined in this section. For an SOFC system such as in Fig. 1 with methane as fuel, the fuel utilization U is mathematically defined as [9], [10], [35]

$$U \triangleq 1 - \frac{\dot{N}_o(4\mathcal{X}_{\text{CH}_4,a} + \mathcal{X}_{\text{CO},a} + \mathcal{X}_{\text{H}_2,a})}{\dot{N}_{\text{in}}(4\mathcal{X}_{\text{CH}_4,r} + \mathcal{X}_{\text{CO},r} + \mathcal{X}_{\text{H}_2,r})} \tag{1}$$

where $\mathcal{X}_{\text{CH}_4,a}$, $\mathcal{X}_{\text{CO},a}$, and $\mathcal{X}_{\text{H}_2,a}$ and $\mathcal{X}_{\text{CH}_4,r}$, $\mathcal{X}_{\text{CO},r}$, and $\mathcal{X}_{\text{H}_2,r}$ are the molar concentrations of CH_4, CO, and H_2 in the anode and the reformer, respectively, and $\dot{N}_o$ and $\dot{N}_{\text{in}}$ are shown in Fig. 1. Based on the molar balance equations and the rate of electrochemical reaction, a steady-state relationship of U can be obtained as in (2), where all the variables and parameters are defined in the Nomenclature section. The derivation is shown in [12] and [37]

$$U = \frac{1-k}{(4nF\dot{N}_f / i_{\text{fc}}\mathcal{N}_{\text{cell}}) - k}. \tag{2}$$

For a desired steady-state utilization U_{ss} and a given demanded FC current $i_{\text{fc},d}$, a fuel flow demand $\dot{N}_{f,d}$ can be calculated from (2), given by

$$\dot{N}_{f,d} = \frac{i_{\text{fc},d}\mathcal{N}_{\text{cell}}}{4nFU_{\text{ss}}}[1 - (1 - U_{\text{ss}})k]. \tag{3}$$

Note that as shown in Fig. 1, the FSS provides fuel flow $\dot{N}_f$ in response to the demand $\dot{N}_{f,d}$, and (3) ensures that at steady state, $U = U_{\text{ss}}$. However, during transience, due to

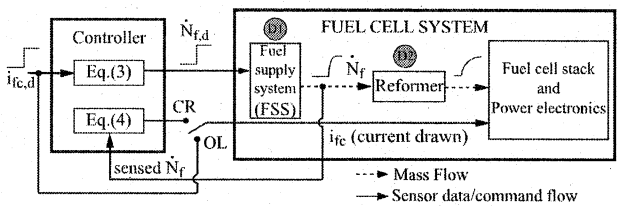

Fig. 2. Transient control of U through CR.

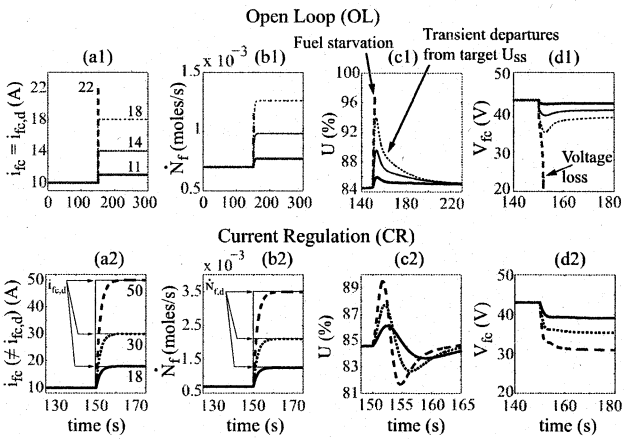

Fig. 3. Simulations showing the transient control of U (from [13]).

the lag associated with the FSS, $\dot{N}_{f,d} \neq \dot{N}_f$. This results in fluctuations in U around U_{ss}. Large changes in $i_{\text{fc},d}$ can result in hydrogen starvation ($U \rightarrow 100\%$). This is illustrated through the simulation results shown in Fig. 3(a1)–(d1). It is mainly attributed to a delay $D1$ (see Fig. 2 and the explanation below) introduced by the FSS between the demanded and actual fuel flows, $\dot{N}_{f,d}$ and $\dot{N}_f$, respectively. This delay can be of the order of a few or several seconds. To address this issue, we propose the CR method by reversing (3) to calculate the regulated current based on the actual fuel flow $\dot{N}_f$ given by

$$i_{\text{fc}} = \frac{4nFU_{\text{ss}}\dot{N}_f}{\mathcal{N}_{\text{cell}}} \frac{1}{[1 - (1 - U_{\text{ss}})k]}. \tag{4}$$

This CR approach as well as lags associated with fuel flow are shown in Fig. 2 with the switch position labeled CR. In comparison, the open-loop (OL) (i.e., unregulated current) approach corresponds to the switch position OL.

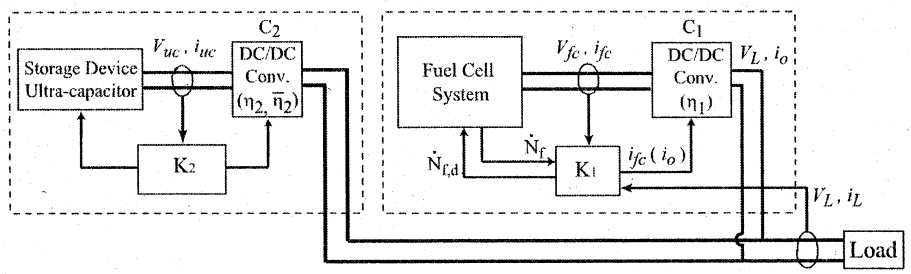

Fig. 4. Schematic of hybrid FC system under decentralized power management.

The proposed CR method has similarities with existing model-based approaches for Polymer Electrolyte Membrane Fuel Cell and SOFC systems using a current filter or a load governor [14], [16], [38]. However, an advantage of CR is that it assumes no knowledge of the dynamic characteristics of the FSS. Improvement in transient response of U in CR over OL is shown in Fig. 3. Details of the simulations and the model can be found in [12] and [13]. As shown, CR allows significantly greater fluctuations in load compared with OL [Fig. 3(a1) and (a2)] before the onset of fuel starvation [Fig. 3(c1) and (c2)]. However, this approach also creates a disparity between $i_{\mathrm{fc},d}$ and i_{fc} during transients [see Fig. 3(a2)]. This implies that while CR protects the FC from fuel starvation due to power fluctuations, it results in a disparity between the demanded and delivered power during transients. This disparity amounts to deficient load following that is addressed by hybridizing the FC with an ultracapacitor. The hybrid system is described next.

C. Hybrid System and Control Objectives

A schematic showing the hybrid FC and the control interface is shown in Fig. 4. Similar as well as alternate methods of interfacing FCs and battery/ultracapacitors can be found in [13], [18], and [39]–[42]. In this configuration, the FC and ultracapacitor are connected in parallel. The FC supplies power to the load through a unidirectional dc/dc converter C_1. The ultracapacitor is connected to the load through a bidirectional dc/dc converter C_2 allowing charge and discharge. Some salient features of the hybrid system are as follows.

1) Due to their fast responses, C_1 and C_2 are assumed to be static energy conversion devices, with C_1 having an efficiency of η_1 and C_2 having discharge and charge efficiencies of η_2 and $\bar{\eta}_2$, respectively [5]. These efficiencies are bounded, but unknown and time varying. We also assume that $\eta_{2,\min} \leq \eta_2, \bar{\eta}_2 \leq (1/\eta_{2,\min})$, and $\eta_{2,\min}$ is known. Furthermore, we consider C_1 function in current control mode, while C_2 maintains voltage V_L in a voltage control mode.
2) Based on the schematic in Fig. 4, since the FC and the ultracapacitor are connected in parallel, the following is true at any instant:

$$V_L i_L = \eta_1 V_{\mathrm{fc}} i_{\mathrm{fc}} + \left[\frac{\eta_2 + \bar{\eta}_2}{2} + \frac{\eta_2 - \bar{\eta}_2}{2}\mathrm{sgn}(i_{\mathrm{uc}})\right] V_{\mathrm{uc}} i_{\mathrm{uc}}$$

$$\Rightarrow \begin{cases} V_L i_L = \eta_1 V_{\mathrm{fc}} i_{\mathrm{fc}} + \eta_2 V_{\mathrm{uc}} i_{\mathrm{uc}}, & i_{\mathrm{uc}} > 0 \\ V_L i_L = \eta_1 V_{\mathrm{fc}} i_{\mathrm{fc}} + \bar{\eta}_2 V_{\mathrm{uc}} i_{\mathrm{uc}}, & i_{\mathrm{uc}} < 0 \end{cases} \quad (5)$$

where $i_{\mathrm{uc}} > 0$ and $i_{\mathrm{uc}} < 0$ imply discharge and charge currents, respectively, of the capacitor. The above equation implies that the net power demand $V_L i_L$ is supplied at every instant. It is also important to note that due to a reversal in the direction of power flow between charge and discharge, for discharge η_2 satisfies $0 < \eta_2 < 1$, while for charge $\bar{\eta}_2$ satisfies $\bar{\eta}_2 > 1$.

3) To realize a decentralized control, we impose the following restrictions on K_1 and K_2. Controller K_1 uses measurements of V_{fc}, V_L, i_L, and $\dot{N}_f$, commands C_1 to draw i_{fc},[1] and commands the FSS to deliver a desired fuel flow rate of $\dot{N}_{f,d}$. However, K_1 does not use measurements of i_{uc}, V_{uc}, η_2, and $\bar{\eta}_2$. This is also indicated in Fig. 4.
4) As shown in Fig. 4, controller K_2 measures V_{uc} and i_{uc} only and does not use measurements of V_L, i_L, V_{fc}, i_{fc}, or η_1. K_2 commands C_2 to maintain a desired load voltage V_L and, in addition, uses dissipation or voltage regulation to control the ultracapacitor's SOC.

Referring to Fig. 4 and under the operational conditions listed above, the control objectives are as follows.

1) The target fuel utilization at steady state will be $U_{\mathrm{ss}} = 0.8$, and the deviations from U_{ss} during transients should be minimized [12], [13].
2) The SOC of the ultracapacitor will be maintained at a target value of $S_t = 0.8$.
3) The load voltage V_L around a nominal value will be controlled.

III. Decentralized Power Management Using Conservation of Energy

A. Approach

This work applies conservation of energy to develop decentralized control of the hybrid system in Fig. 4. Conceptually, the approach is shown in Fig. 5. Fig. 5 shows a step change in power demand $V_L i_L$ and the corresponding load-following response of the source (FC, $\eta_1 V_{\mathrm{fc}} i_{\mathrm{fc}}$). In load-following mode, the SOFC's delivered power $\eta_1 V_{\mathrm{fc}} i_{\mathrm{fc}}$ will track the load demand $V_L i_L$, meeting the demand exactly at steady state. Equation (5) is satisfied at all times. In addition, at steady state, the load $V_L i_L$ is constant and $V_L i_L = \eta_1 V_{\mathrm{fc}} i_{\mathrm{fc}} \Rightarrow i_{\mathrm{uc}} = 0$. In Fig. 5, the intervals $t < t_0$ and $t > t_f$ represent the steady-state conditions.

[1] In implementation, hardware limitations require K_1 to command i_o instead of i_{fc}, as described in Section IV-B1.

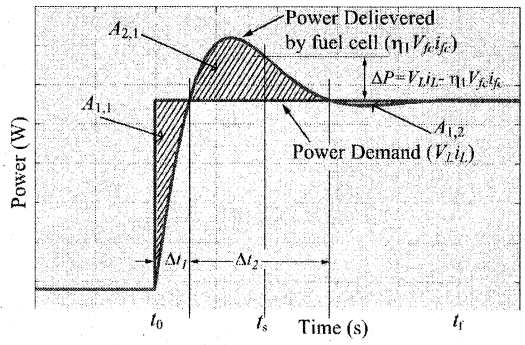

Fig. 5. Conservation of energy approach.

Next, we discuss the transient region of the plot, namely, the interval $t_0 \leq t \leq t_f$. This region captures how the SOFC responds to the load change. The response shown in Fig. 5 is a sample to show the energy-conservation-based approach. Consider an arbitrary instant t_s as shown. We define ΔP to be the instantaneous difference between the load and delivered power. Hence, ΔP as shown in Fig. 5 is

$$\Delta P \triangleq V_L i_L - \eta_1 V_{\text{fc}} i_{\text{fc}}. \tag{6}$$

We will use this definition to formulate the energy-conservation-based decentralized control. Also note that the shaded area $A_{1,1}$ represents the total deficit between the demand and energy supplied by the SOFC over the interval Δt_1. The area thus represents energy removed from the ultracapacitor (discharged). Similarly, the shaded area $A_{2,1}$ represents an excess energy supplied by the SOFC during the interval Δt_2. Area $A_{2,1}$ thus represents energy returned to the ultracapacitor (charged). From Fig. 5 and (5), we can conclude that

$$\begin{aligned} A_{1,1} &= \int_{t_0}^{t_0+\Delta t_1} \Delta P\, dt = \int_{t_0}^{t_0+\Delta t_1} (V_L i_L - \eta_1 V_{\text{fc}} i_{\text{fc}}) dt \\ &= \int_{t_0}^{t_0+\Delta t_1} \eta_2 V_{\text{uc}} i_{\text{uc}} dt \\ A_{2,1} &= \int_{t_0+\Delta t_1}^{t_0+\Delta t_1+\Delta t_2} -\Delta P\, dt \\ &= \int_{t_0+\Delta t_1}^{t_0+\Delta t_1+\Delta t_2} -(V_L i_L - \eta_1 V_{\text{fc}} i_{\text{fc}}) dt \\ &= \int_{t_0+\Delta t_1}^{t_0+\Delta t_1+\Delta t_2} -\bar{\eta}_2 V_{\text{uc}} i_{\text{uc}} dt. \end{aligned} \tag{7}$$

In the transient response of the SOFC, we denote $A_{1,j}$, $j = 1, 2, \ldots$, by the areas where the ultracapacitor is discharged and $A_{2,q}$, $q = 1, 2, \ldots$, by the areas where the ultracapacitor is charged. Then under ideal charge/discharge, i.e., $\eta_2 = \bar{\eta}_2 = 1$, the condition

$$\lim_{t\to\infty} E_A = \lim_{t\to\infty} \left(\sum_j A_{1,j} - \sum_q A_{2,q} \right) \to 0 \tag{8}$$

will ensure that at steady state $t > t_f$, the energy of the ultracapacitor, i.e., its SOC, will be preserved at the same value as in the previous steady state $t < t_0$. Equation (8) can be generalized to the following integral condition:

$$\lim_{t\to\infty} E_A = \lim_{t\to\infty} \int_{t_0}^{t} \Delta P\, dt = 0. \tag{9}$$

Essentially, controller K_1 that controls the delivered FC power can satisfy this integral condition by simply modulating the cell-side power, with no information about the ultracapacitor's SOC. This is because ΔP is only a function of V_{fc}, i_{fc}, and η_1 that are all local information and V_L and i_L that are commonly available. However, (9) is an ideal scenario where there are no losses in the charge/discharge processes. In the presence of charge/discharge losses in C_2, with discharge and charge efficiencies η_2 and $\bar{\eta}_2$, respectively, (8) must be modified to

$$\lim_{t\to\infty} E_A = \lim_{t\to\infty} \left(\sum_j \frac{A_{1,j}}{\eta_2} - \sum_q \frac{A_{2,q}}{\bar{\eta}_2} \right) \to 0. \tag{10}$$

The above equation is obtained from (5) and (8), and is obvious if we remove the assumption $\eta_2 = \bar{\eta}_2 = 1$ from (7). If we assume η_2 and $\bar{\eta}_2$ to be nonunity but known, (10) can be generalized to the following integral condition that can be satisfied by controller K_1:

$$\begin{aligned} &\lim_{t\to\infty} E_A \\ &= \lim_{t\to\infty} \int_{t_0}^{t} \left[\frac{\eta_2^{-1} + \bar{\eta}_2^{-1}}{2} + \frac{\eta_2^{-1} - \bar{\eta}_2^{-1}}{2} \text{sgn}(\Delta P) \right] \Delta P dt \to 0. \end{aligned} \tag{11}$$

Here sgn(.) represents the signum function. However, η_2 and $\bar{\eta}_2$ will be unknown to K_1. Therefore, we need to build a robust control around this principle to handle the uncertainty in a decentralized manner. The next section will demonstrate the validity of the main principle outlined in this section.

B. Simulations

To demonstrate that energy conservation can be used to design decentralized control, we consider a simplified scenario. We assume that in addition to the local information mentioned in Section II-C, controller K_1 has knowledge of η_2 and $\bar{\eta}_2$. This assumption will be removed in latter sections. Next, we note from Fig. 4 that controller K_1 generates two control inputs, i_{fc} and $\dot{N}_{f,d}$. The inputs, generated using (3) and (4), implement CR for transient control of U (see Fig. 2). The design of $i_{\text{fc},d}$ is based on the following observation: in load-following mode, the SOFC's delivered power $\eta_1 V_{\text{fc}} i_{\text{fc}}$ tracks the load demand $V_L i_L$, meeting the demand exactly at steady state. Additional perturbations in $\eta_1 V_{\text{fc}} i_{\text{fc}}$ will be introduced to achieve (11). With this goal and incorporating the approach outlined in Section III-A, we formulate $i_{\text{fc},d}$ as

$$i_{\text{fc},d} = \frac{V_L i_L + g_i E_A}{\eta_1 V_{\text{fc}}}, \quad g_i > 0 \tag{12}$$

where g_i is an integral gain, and E_A is defined in (11) and can be calculated by K_1 using local information only.

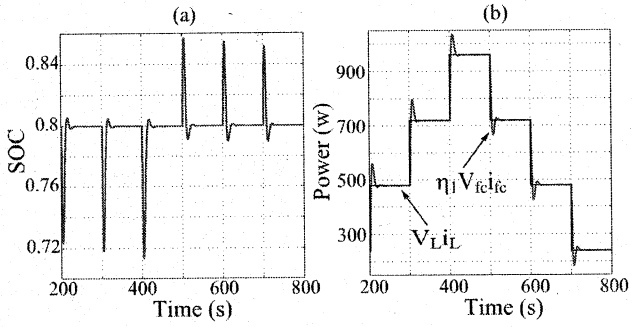

Fig. 6. Energy-conservation-based control with known η_2 and $\bar{\eta}_2$.

Controller K_2 simply maintains constant voltage V_L (in this case, 24 V) across the load. The design is implemented and simulation results are summarized in Fig. 6. The parameter values chosen are

$$C = 25\text{F}, \eta_1 = 0.8, \eta_2 = \bar{\eta}_2 = 0.8$$
$$g_i = 4, S_t = 0.8, U_{ss} = 0.8. \tag{13}$$

The power demand $V_L i_L$ is subjected to step changes, as shown in Fig. 6(b). Fig. 6(a) confirms the control of SOC and Fig. 6(b) plots $V_L i_L$ and $\eta_1 V_{fc} i_{fc}$. The excursions of $\eta_1 V_{fc} i_{fc}$ from $V_L i_L$, as it fluctuates, are such that $\lim_{t\to\infty} E_A = 0$. The assumption in this section that K_1 has exact knowledge of η_2 and $\bar{\eta}_2$ is quite restrictive. In the next section, we relax this assumption by treating the efficiencies as unknowns. Further, we augment the main approach of Section III-A with a dissipation mechanism to introduce robustness.

C. Robust Performance Through Dissipation

1) Design of K_1 Using a Lower Bound $\eta_{2,min}$ of η_2 and $\bar{\eta}_2$: We now consider a more realistic case where controller K_1 has no knowledge of η_2 and $\bar{\eta}_2$ but only knows a lower bound $\eta_{2,\min} \le \eta_2, \bar{\eta}_2 \le (1/\eta_{2,\min})$. Accordingly, $i_{fc,d}$ in (12) must be formulated with E_A as shown in the following instead of (11):

$$E_A \triangleq \int_{t_0}^{t} \left[\frac{\eta_{2,\min}^{-1} + \eta_{2,\min}}{2} + \frac{\eta_{2,\min}^{-1} - \eta_{2,\min}}{2} \text{sgn}(\Delta P) \right] \Delta P dt. \tag{14}$$

Note that (14) uses conservative estimates of the magnitudes of discharge and charge. Specifically, it estimates higher discharge and lower amount of charge. The expected result is that by ensuring $\lim_{t\to\infty} E_A = 0$, it is guaranteed that the ultracapacitor will be overcharged for every step change in $V_L i_L$. Next, we observe that (3), (4), (12), and (14) generate a feedback loop. Our objective is to investigate the stability of the equilibrium $\Delta P = 0$ of this closed-loop system and show that indeed at steady state $E_A = 0$. We next state the following assumption about the FSS. Defining the error between the actual and demanded fuel flow rates as $E_{fl} = \dot{N}_f - \dot{N}_{f,d}$, we assume that $E_{fl}(t)$ satisfies a general exponential decay condition given by

$$|E_{fl}(t)| \le \gamma |E_{fl}(t_0)| e^{-\zeta(t-t_0)} \quad \forall\, |E_{fl}(t_0)| < r_0 \tag{15}$$

where $\gamma, \zeta, r_0 > 0$ are constants. This is valid because the FSS causes $\dot{N}_f$ to track $\dot{N}_{f,d}$. Then it can be shown that the error variable $E_{fc,d} = i_{fc} - i_{fc,d}$ satisfies

$$|E_{fc,d}(t)| \le \gamma |E_{fc,d}(t_0)| e^{-\zeta(t-t_0)} \quad \forall\, |E_{fc,d}(t_0)| < r_0/\beta \tag{16}$$

where $\beta = (\mathcal{N}_{cell}/4nFU_{ss})[1 - (1 - U_{ss})k]$ is a positive constant. The proof of this result is simple and details can be found in [13]. We note here that the FSS behavior of (15) is not restrictive and common responses such as first-order or ramped behavior can be bounded by exponential decay. Next, we state and prove the following theorem.

Theorem 1: If the FSS satisfies the generalized behavior of (15), then for step changes in i_L, the design of controller K_1 consisting of (3), (4), (12), and (14) renders the equilibrium $\Delta P = 0$ asymptotically stable and ensures $\lim_{t\to\infty} E_A = 0$.

Proof: Equation (12) can be rearranged to

$$\Delta P_d + g_i E_A = 0, \quad \text{where} \quad \Delta P_d = V_L i_L - \eta_1 V_{fc} i_{fc,d}. \tag{17}$$

Taking the derivative of (17) and from (14), we get

$$\frac{d}{dt}(\Delta P_d) + g_i \alpha \Delta P = 0, \text{ where } \alpha = \begin{cases} \eta_{2,\min}^{-1} & \text{for } \Delta P > 0 \\ \eta_{2,\min} & \text{for } \Delta P < 0. \end{cases} \tag{18}$$

Also note from (6), (17), and (18) that

$$\begin{aligned} \Delta P &= \Delta P_d - \eta_1 V_{fc} E_{fc,d} \\ &\Rightarrow \frac{d}{dt}(\Delta P_d) + g_i \alpha (\Delta P_d - \eta_1 V_{fc} E_{fc,d}) = 0. \end{aligned} \tag{19}$$

Further, we observe from (16) and *converse Lyapunov theorems* [43] that there exists a positive definite function $\bar{V}_{fc}$ and the constants α_1, α_2, and α_3 such that

$$\begin{aligned} &\alpha_1 E_{fc,d}^2 \le \bar{V}_{fc}(E_{fc,d}, t) \le \alpha_2 E_{fc,d}^2 \\ &\qquad 0 < \alpha_1 < \alpha_2 \quad \text{and} \quad \dot{\bar{V}}_{fc} \le -\alpha_3 E_{fc,d}^2, \quad \alpha_3 > 0. \end{aligned} \tag{20}$$

Then considering the Lyapunov function candidate $V = (1/2)(\Delta P_d^2) + \lambda \bar{V}_{fc}$, $\lambda > 0$ being a constant, and differentiating V with respect to time produces

$$\begin{aligned} \dot{V} &\le \Delta P_d \frac{d}{dt}(\Delta P_d) - \lambda \alpha_3 E_{fc,d}^2 \\ &\le -g_i \alpha \Delta P_d^2 - \lambda \alpha_3 E_{fc,d}^2 + g_i \alpha \eta_1 V_{fc} E_{fc,d} \Delta P_d \\ &\le -\mathcal{E}^T Q \mathcal{E} < 0 \\ \mathcal{E} &= \begin{bmatrix} \Delta P_d \\ E_{fc,d} \end{bmatrix}, \; Q = \begin{bmatrix} g_i \alpha & -0.5 g_i \alpha \eta_1 V_{fc} \\ -0.5 g_i \alpha \eta_1 V_{fc} & \lambda \alpha_3 \end{bmatrix}. \end{aligned}$$

Note that Q is symmetric and, in addition, λ can be chosen to ensure that Q is positive definite. Thus, $\dot{V}$ will be negative definite and the equilibrium $\mathcal{E} = [\mathbf{0}]$ is asymptotically stable (in fact, exponentially stable since Q is positive definite and symmetric [44]). From (17) and (19), we then conclude that at equilibrium (steady state)

$$\mathcal{E} = [\mathbf{0}] \Rightarrow \Delta P_d, E_{fc,d} = 0 \Rightarrow \Delta P, E_A = 0.$$

This completes the proof. ■

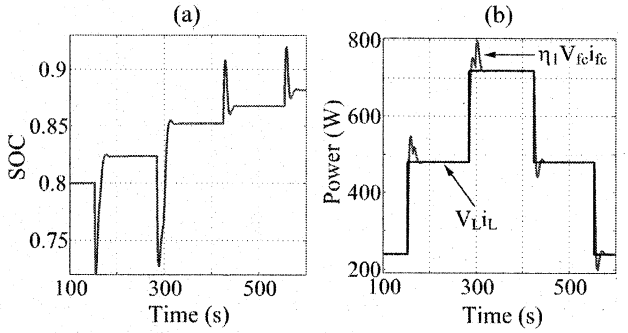

Fig. 7. Energy conservation with a conservative estimate $\eta_{2,\min}$ of η_2 and $\bar{\eta}_2$.

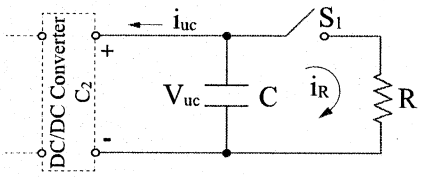

Fig. 8. Dissipation circuit.

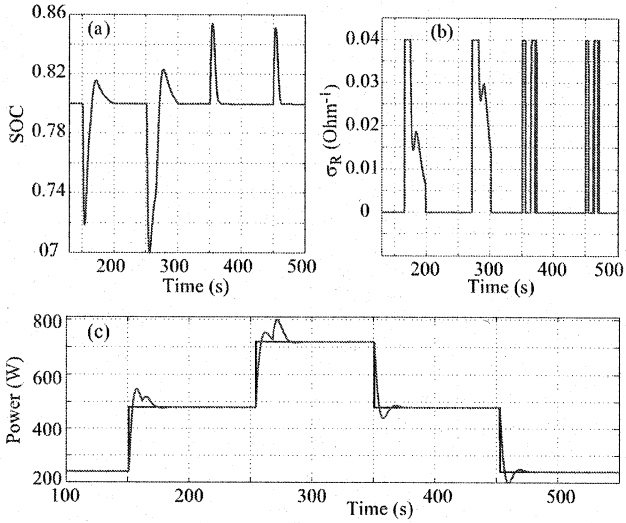

Fig. 9. System response with a PI controller for dissipation.

Simulation results with E_A calculated using (14) are shown in Fig. 7. The parameter values chosen were the same as those in (13). In addition, $\eta_{2,\min} = 0.7$ was chosen. The formulation of E_A according to (14) is conservative, as mentioned earlier in this section. The conservative nature of this approach is evident in Fig. 7(a) where the SOC increases with power fluctuations. The power demand $V_L i_L$ and SOFC's supplied power $\eta_1 V_{fc} i_{fc}$ are plotted together in Fig. 7(b). Since we consider a energy storage device of finite capacity, its SOC must be regulated. To address this regulation in a decentralized manner, we incorporate dissipation in controller K_2, as discussed in Section III-C2.

We end this section by noting that the performance of K_1 can also be viewed from a classical controls perspective, under certain simplifications. In (16), if we assume equality instead of the inequality, then we can write $\dot{E}_{fc,d} = -\zeta E_{fc,d}$. In addition, in (18), if we assume small changes in V_{fc}, then the overall closed-loop dynamics can be expressed as

$$\frac{d^2}{dt^2}(\Delta P_d) + (g_i\alpha + \zeta)\frac{d}{dt}(\Delta P_d) + g_i\alpha\zeta(\Delta P_d) = 0.$$

From this linear dynamical equation, we can estimate the bandwidth of the closed-loop system to be $\omega_{bw} \approx (g_i\alpha\zeta)^{1/2}$. Since α can switch between $\eta_{2,\min}^{-1}$ and $\eta_{2,\min}$, a conservative estimate would be $\omega_{bw} \approx (g_i\eta_{2,\min}\zeta)^{1/2}$. Furthermore, the term $(g_i\alpha + \zeta)$ provides an approximate damping of the closed-loop system. However, it must be recognized that the original dynamics is nonlinear, and hence, these predictions can be substantially off.

2) Dissipation-Based Design of K_2: In this approach, the ultracapacitor's SOC is regulated via dissipation through a variable resistance. We add a resistance in parallel with a capacitor, which is shown in Fig. 8. Energy dissipation is controlled by K_2 by actuating a pulsewidth-modulated switch S_1, shown in Fig. 8. Since SOC is a local information for K_2, charge management is done locally without any information about the FC from K_1. The circuit equation corresponding to Fig. 8 is

$$C\dot{V}_{uc} = -(i_{uc} + i_R), \quad \dot{V}_{uc} = -\frac{1}{C}(i_{uc} + V_{uc}\sigma_R) \tag{21}$$

where σ_R is the effective conductance that can be varied by changing the duty cycle of S_1. We treat σ_R as a control input and use the following control law to stabilize the equilibrium $V_{uc} = V_{uc,d}$:

$$\sigma_R = \frac{g_{p,uc}}{V_{uc}}(V_{uc} - V_{uc,d}) + \frac{g_{i,uc}}{V_{uc}}\int_0^t (V_{uc} - V_{uc,d})\,dt$$
$$\begin{cases} \dot{\sigma}_R = 0, & \text{if } \sigma_R = \sigma_{R,\max} \text{ and } V_{uc} > V_{uc,d} \\ \sigma_R = \dot{\sigma}_R = 0, & \text{if } V_{uc} \le V_{uc,d} \end{cases} \tag{22}$$

where $g_{p,uc}$ and $g_{i,uc}$ are proportional and integral gains, respectively, and $V_{uc,d}/V_{uc,\max} = S_t$, the target SOC. $V_{uc,\max}$ is the known ultracapacitor voltage at which its SOC is 100%. The efficacy of this controller is shown through simulation results in Fig. 9. The manner in which the resistance R is used in the proportional–integral (PI) control is evident from Fig. 9(b). For this simulation, $S_t = 0.8$ and $V_{uc,\max} \approx 16$ V, and hence, $V_{uc,d} = 13$ V. In addition, $g_{p,uc} = 0.08$ and $g_{i,uc} = 0.0016$. We assume $R = 25\ \Omega$ and that σ_R linearly varies with duty cycle $= 0 \Rightarrow \sigma_R = 0$, to duty cycle $= 1 \Rightarrow \sigma_R = 0.04$. In contrast to Fig. 7(a) where the SOC control was not implemented in K_2, the SOC converges to $S_t = 0.8$ with the control law of (22).

The performance of the SOC controller can be studied in frequency domain (transfer functions) since both the ultracapacitor and the PI controller in (21) and (22) are linear systems [45]. Defining the error $E_{uc} = V_{uc} - V_{uc,d}$ and taking Laplace transforms under zero initial conditions, we get the following closed-loop equation:

$$E_{uc}(s) = \frac{-V_{uc,d}(s)}{1 + \frac{1}{Cs}\left(g_{p,uc} + \frac{g_{i,uc}}{s}\right)} - \frac{(1/Cs)i_{uc}(s)}{1 + \frac{1}{Cs}\left(g_{p,uc} + \frac{g_{i,uc}}{s}\right)}.$$

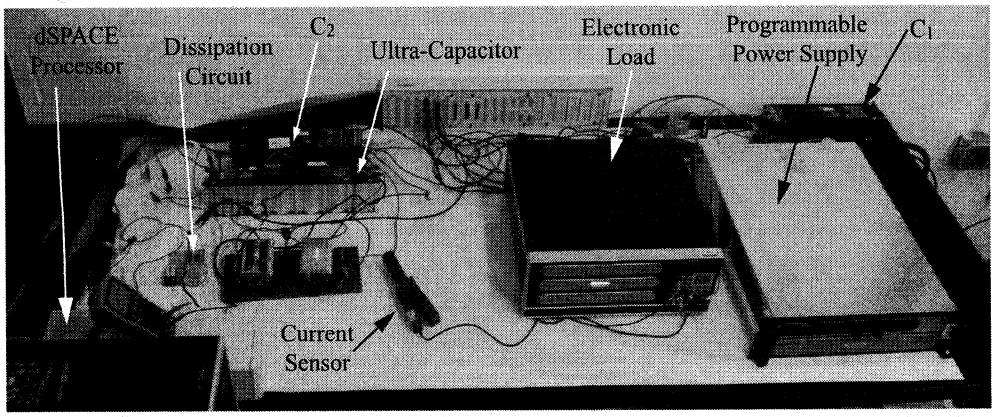

Fig. 10. Experimental test stand.

Note that the above closed-loop system with the characteristic equation $Cs^2 + g_{p,\mathrm{uc}}s + g_{i,\mathrm{uc}} = 0$, and positive $g_{p,\mathrm{uc}}$ and $g_{i,\mathrm{uc}}$ is stable. In addition, the system is type-2 with respect to $V_{\mathrm{uc},d}$ and type 1 with respect to i_{uc}. Since $V_{\mathrm{uc},d}$ is a constant and i_{uc} is zero at steady state, reference tracking and disturbance rejection are simultaneously achieved by the PI controller proposed in (22). Thus, $E_{\mathrm{uc}} = 0$ at steady state. The low-pass characteristics of the loop gain transfer function $L(s) = (1/Cs)(g_{p,\mathrm{uc}} + (g_{i,\mathrm{uc}}/s))$ gives the controller its desired reference tracking and disturbance rejection abilities [45]. Note that the controller does not attempt to cancel i_{uc} through feedback, but instead treats it as a disturbance signal. This is because in load-following mode and at steady state, $V_L i_L = \eta_1 V_{\mathrm{fc}} i_{\mathrm{fc}}$ and hence $i_{\mathrm{uc}} = 0$. Hence, the noise-to-signal ratio in measured i_{uc} is expected to be high, and sensor-based cancellation of i_{uc} will introduce extra noise in the feedback loop. We end this section with the following observation.

Remark 1: Controllers K_1 and K_2, discussed in Sections III-C1 and III-C2, perform independently of each other. The stability characteristics of either closed-loop system do not affect those of the other.

IV. Experimental Setup and Results

A. Experimental Setup

The theoretical framework developed for decentralized control is validated using experimental setup. The experimental hardware-in-the-loop setup consists of the emulated FC along with an ultra capacitor, an electronic load, and two dc–dc converters. The setup is shown in Fig. 10. The technical specification of each equipment is given in Table I. More details of the setup can be found in [13]. The FC system that is employed is a real-time emulation of a mathematical model of the SOFC developed in [12]. Before discussing results, we summarize some aspects of practical implementation that posed challenges.

B. Details of Practical Implementation

1) Control of Unidirectional Converter C_1: As mentioned in Section II and also evident from the development in Sections III and III-C1, the dc/dc converter C_1 (see Fig. 4) is controlled in current control mode. To apply our theory directly, K_1 must command C_1 to deliver i_{fc}. However, referring to Fig. 4, the converter C_1 in our setup allows us only to command i_o directly and not i_{fc}. Hence, in Fig. 4 and Section II-C, we indicate i_o to be the input to C_1 in the hardware. The dc/dc converter has an in-built controller that takes a sensed feedback of i_o flowing through a Hall-effect sensor inside the converter and, using a PI controller, precisely tracks the reference value set by the user at the control terminal. To circumvent this hardware limitation, we propose the following feedforward and feedback combination:

$$i_o = \frac{\eta_1 V_{\mathrm{fc}} i_{\mathrm{fc,cal}}}{V_L} + g_{p,o} E_{\mathrm{fc,cal}} + g_{i,o} \int_0^t E_{\mathrm{fc,cal}} dt$$
$$E_{\mathrm{fc,cal}} \triangleq i_{\mathrm{fc,cal}} - i_{\mathrm{fc}}. \tag{23}$$

Here, we treat (4) to provide a calculated current $i_{\mathrm{fc,cal}}$, i.e., $i_{\mathrm{fc,cal}} = 4nFU_{\mathrm{ss}}\dot{N}_f/(\mathcal{N}_{\mathrm{cell}}[1-(1-U_{\mathrm{ss}})k])$, while i_{fc} is the measured current. The objective of (23) is then to ensure $\lim_{t\to\infty} E_{\mathrm{fc,cal}} = 0$. In (23), $g_{p,o}$ and $g_{i,o}$ are the positive proportional and integral gains. The internal controller in C_1 generates fast response, on the order of microseconds. Hence, it is reasonable to assume that i_o generated by (23) is instantaneously achieved at the output of C_1. The feedforward term $(\eta_1 V_{\mathrm{fc}} i_{\mathrm{fc,cal}}/V_L)$ in (23) comes from the power balance at the input and output terminals of the converter C_1. The sequence of signal flow is explained through the schematic in Fig. 11. We next state and prove the following theorem.

TABLE I
Equipment Specifications

Item	Spec.(V)	Spec.(i)	Make
dSpace	-	-	dSpace1103
Power Supply	110V AC/DC	o/p:50A	Ametek SGA100/50
Electronic Load	i/p:120V AC	0-120A	Sorenson SLH
Ultracapacitor(250F)	16.2V DC	2000A	BMOD0250 P16
Unidirectional Converter C_1	44-50V DC	40A	Zahn DC-5050F-SU
Bidirectional Converter C_2	44-50V DC	40A	Zahn DC-5050F-SU
Current Sensors	-	1-100A	Fluke-80i-110S

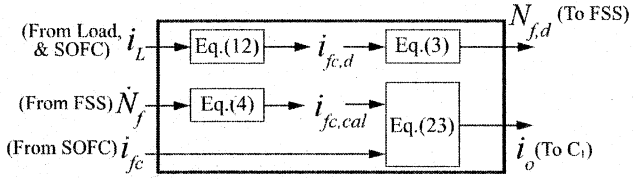

Fig. 11. Schematic of signal flow in K_1.

Theorem 2: The control law given in (23) leads to exponential convergence of $E_{\text{fc,cal}} \to 0$ for $g_{p,o} > 0$ and $g_{i,o} > 0$.

Proof: To prove this, we assume that the change in the feedforward term $(\eta_1 V_{\text{fc}} i_{\text{fc,cal}}/V_L)$ in (23) is small during the correction interval, which is reasonable if $g_{p,1}$ and $g_{i,1}$ are assigned relatively high values. Referring to Fig. 11, we then have

$$\frac{di_o}{dt} = \frac{\eta_1 V_{\text{fc}}}{V_L}\frac{di_{\text{fc}}}{dt} = g_{p,o}\dot{E}_{\text{fc,cal}} + g_{i,o}E_{\text{fc,cal}}$$
$$\Rightarrow \left(g_{p,o} + \frac{\eta_1 V_{\text{fc}}}{V_L}\right)\dot{E}_{\text{fc,cal}} + g_{i,o}E_{\text{fc,cal}} = 0. \quad (24)$$

Using a Lyapunov function $V = E_{\text{fc,cal}}^2$ and (24), it is easy to verify that $E_{\text{fc,cal}}$ converges to zero exponentially, provided that $g_{p,o} > 0$ and $g_{i,o} > 0$ [43]. ■

2) η_1 Measurement: It has been assumed throughout this paper that the measurement of η_1 is available to K_1, since it is a local variable. In our experimental setup, it is measured by implementing the power balance equation for C_1, which is $V_L i_o = \eta_1 V_{\text{fc}} i_{\text{fc}}$. Since V_{fc}, i_{fc}, and V_L are measured and i_o is a command, a coarse measurement of η_1, namely, $\eta_{1,m} = V_L i_o / V_{\text{fc}} i_{\text{fc}}$, is first obtained. The measured value is then filtered to obtain η_1. This approach gave satisfactory control validation results.

3) PWM Switching Circuit: Referring to Fig. 8, controller K_2 manipulates the duty ratio μ to change the dissipation rate as follows:

$$\mu(t) = \frac{g_{p,\text{uc}}}{V_{\text{uc}}}(V_{\text{uc}} - V_{\text{uc},d}) + \frac{g_{i,\text{uc}}}{V_{\text{uc}}}\int_0^t (V_{\text{uc}} - V_{\text{uc},d})\,\text{d}t$$
$$\begin{cases} \dot{\mu} = 0, \text{ if } \mu = 1 \text{ and } V_{\text{uc}} > V_{\text{uc},d} \\ \mu = \dot{\mu} = 0, \text{ if } V_{\text{uc}} \le V_{\text{uc},d} \end{cases} \quad \sigma_R = \mu\sigma_{R,\max}. \quad (25)$$

The average voltage appearing across the dissipating resistor effectively determines i_R. The relation between the duty ratio $\mu(t)$ and i_R can be formulated as

$$\frac{1}{T}\int_0^T V_{\text{uc}}\,\mu(t)dt = i_R R$$

where $1/T$ is the switching frequency of the PWM. The PWM circuit is switched OFF as soon as the equilibrium $V_{\text{uc}} = V_{\text{uc},d}$ is established. The hardware consists of a simple solid-state switch that drives the gate of a power MOSFET of appropriate rating whenever the ultracapacitor voltage surpasses a certain threshold voltage. The voltage reference is set to $V_{\text{uc},d} = 12.2$ V above which the PWM circuit activates. Moreover, the rate of discharge is controlled by the pulsewidth of the PWM signal that is realized by driving the gate of the MOSFET. The gate driver circuit consists of *UCC*27322 gate driver IC that can produce a 9-A peak current at the Miller Plateau region of the MOSFET [46]. The schematics and hardware of the PWM circuit are shown in Fig. 12.

4) Bidirectional Converter Control: The bidirectional converter C_2 is operated in voltage control mode. The primary purpose of this converter is to maintain a constant voltage across the load at all times. The converter has been set to maintain $V_L = 23$ V across the load for the dissipation-based method. The choice of this value for V_L is driven by the limiting output voltage of C_2, which is 23.3 V.

C. Experimental Results

The decentralized approach with dissipation-based SOC control, discussed in Sections III and III-C, is tested on the experimental setup and the results are shown in Fig. 13. As shown in Fig. 13(a), a repetitive step load change from 10-A level to 20-A level is implemented. Fig. 13(d) confirms transient fuel utilization control with only an $\approx \pm 2\%$ deviation about the target $U_{\text{ss}} = 80\%$. Fig. 13(b) and (e) is self-explanatory, representing FC current and voltages. Fig. 13(f) compares V_{uc} with (blue) and without (red) dissipation. For the test, we set $S_t = 0.75$, which corresponds to $V_{\text{uc},d} \approx 12.2$ V. The conservative nature of K_1 is clear, since it gradually overcharges the capacitor in the absence of dissipation (in K_2). With controlled dissipation, the issue is addressed.

In the experiment, the controller parameters are chosen as follows: for K_1, $g_i = 0.01$ in (12) and $g_{p,o} = g_{i,o} = 0.01$ in (23), and for K_2, $g_{p,\text{uc}} = 0$ and $g_{i,\text{uc}} = 20$ in (25). In Fig. 13(c), i_{uc} is plotted. As expected, i_{uc} goes to zero at steady state, indicating that, indeed, the FC supplies the entire power demand at steady state. The slow response of the FC to the load changes along with the capacitor's contribution to make up for FC's deficiency during load transients is visible in Fig. 13(g). In Fig. 13(g), also observe that $A_{1,1} < A_{2,1}$. This is due to losses in C_2 that translates to (10) for conserving the capacitor's energy.

V. Robustness Through Voltage Modulation

A. Approach and Simulation Results

Using dissipation for controlling the SOC is a conservative approach that relies on dissipating the excess energy going to the storage element. The idea in the voltage regulation method is to minimize this loss. Note that energy loss would be prevented if the FC controller K_1 has accurate knowledge of η_2 and $\bar{\eta}_2$. Hence, the objective of this design is to develop a mechanism by which K_1 can learn the aforementioned efficiencies without direct sensing or communicating with K_2. As mentioned in Section II-C, K_2 can manipulate V_L. In the proposed voltage modulation approach, K_2 changes V_L as the SOC deviates from S_t. Specifically, V_L is increased from a nominal value of $V_{L,\text{nom}}$, as the capacitor gets gradually overcharged. Since V_L is a global variable, K_1 simultaneously uses changes in V_L to improve its estimates of η_2 and $\bar{\eta}_2$. The process, when designed properly, causes the estimates to eventually settle close to the actual values of η_2 and $\bar{\eta}_2$.

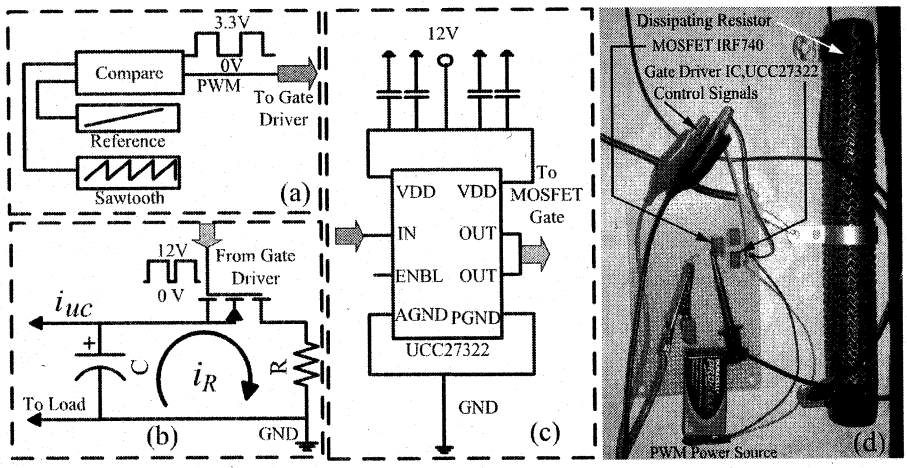

Fig. 12. (a) Schematic of a PWM generator. (b) Discharge crcuit. (c) Gate driver. (d) Switching circuit.

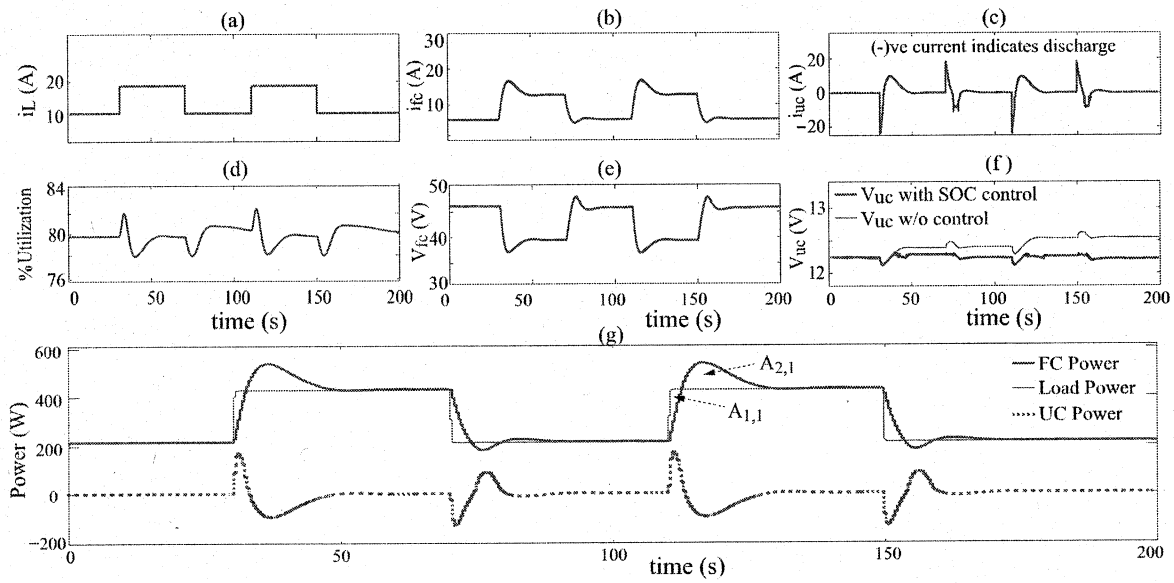

Fig. 13. Experimental results for the dissipation-based approach.

This diminishes overcharging of the ultracapacitor with progress of time. It is emphasized that this paper simply presents the voltage modulation approach as a viable alternate to dissipation. Theoretical analysis of the approach is an area of future research.

Voltage fluctuation is undesirable in power networks. Therefore, the aforementioned modulation method, even though is capable of inducing K_1 to improve its efficiency estimates, must be designed in a way such that voltage fluctuations are low and they diminish over time. We propose V_L to be modulated by K_2 using an integral action

$$V_L = V_{L,\text{nom}} + g_{i,v2} \int_0^t (V_{\text{uc}} - V_{\text{uc},d})dt$$

where $V_{L,\text{nom}}$ is the nominal load voltage and $g_{i,v2}$ is the integral gain. When V_{uc} is sufficiently close to $V_{\text{uc},d}$, the integrator resets V_L to $V_{L,\text{nom}}$. In parallel, an integral action is used in K_1 to utilize the voltage deviations from $V_{L,\text{nom}}$ for efficiency estimation

$$\eta_{2,\min}(t) = \eta_{2,\min}(t_0) + g_{i,v1} \int_0^t (V_L - V_{L,\text{nom}})dt.$$

Simulation results are shown in Fig. 14. In the simulation, pulsed changes in power demand were applied every 200 s. Parameter values were $g_{i,v1} = 0.0005$, $g_{i,v2} = 0.005$, $\eta_2 = \bar{\eta}_2 = 0.8$, and $V_{L,\text{nom}} = 24$ V. From Fig. 14(a), it is clear that K_2 is able to maintain the SOC through voltage modulation. Further, Fig. 14(b) shows that voltage fluctuations reduce over time. This is primarily due to better estimation of $\eta_{2,\min}$ by K_1 over time. The estimation is shown in Fig. 14(c). The saw-tooth type of response, as shown in Fig. 14(b), is due to integrator resets. Another observation is that during higher SOC/voltage fluctuations toward the beginning, efficiency adaptation was faster and it decreased

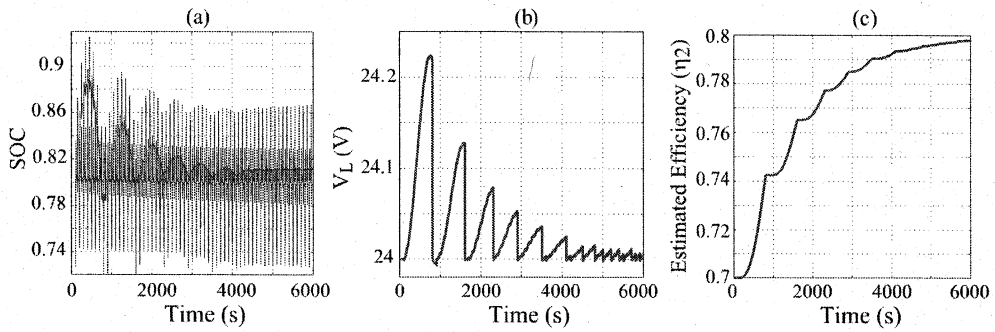

Fig. 14. Simulations with voltage modulation and efficiency estimation.

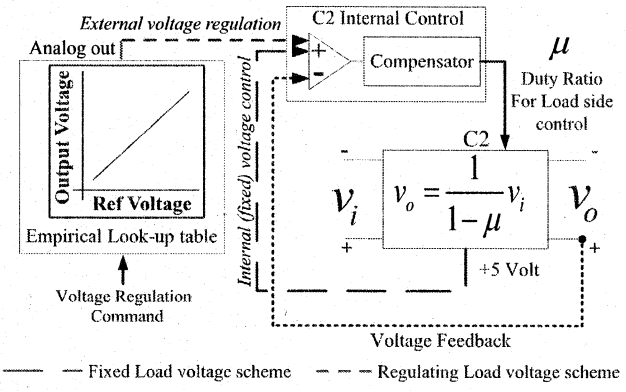

Fig. 15. Implementation of external voltage modulation on C_2.

with time. The estimation process therefore requires not only the voltage modulation but also persistent perturbations in the power demand.

B. Implementation and Experimental Results

Voltage modulation capability was facilitated in the converter C_2 with minor changes to its internal circuitry. Hardware limitations of C_2 limit the maximum $V_{L,\text{nom}}$ to $\approx$23.3 V. Hence, to allow voltage modulation $V_{L,\text{nom}} = 22$ V is chosen in (26). The modifications to C_2 to implement voltage modulation are shown in Fig. 15. Two integrators were used at the SOFC side (i.e., K_1) to utilize the load deviations from 22 V for efficiency estimation, to account for the different discharging and charging efficiencies, namely, η_2 and $\bar{\eta}_2$, respectively

$$\hat{\eta}_2(t) = \hat{\eta}_2(t_0) + g_{i,v11} \int_0^t (V_L - 22)dt$$
$$\dot{\hat{\eta}}_2 = 0, \text{ when discharging}$$
$$\hat{\bar{\eta}}_2(t) = \hat{\bar{\eta}}_2(t_0) + g_{i,v12} \int_0^t (V_L - 22)dt$$
$$\dot{\hat{\bar{\eta}}}_2 = 0, \text{ when charging.}$$

In the experiment, the following parameter values were chosen, $g_{i,v2} = 0.1$, $g_{i,v11} = 0.001$, $g_{i,v12} = 0.002$, and $\hat{\eta}_2(t_0) = \hat{\bar{\eta}}_2(t_0) = 0.7$. The experimental results are shown in Fig. 16.

The power draw was pulsed at regular interval, as shown in Fig. 16(a). Fig. 16(b) shows the main result of the experiment, indicating that load voltage fluctuations imposed by K_2 diminished over time starting from $\sim$0.5 to < 0.05 V. This is because with progressive improvement of the efficiency estimates, the net capacitor overcharge over individual power pulses reduce. The corresponding variations in V_{uc}, i_{uc}, and i_{fc} are shown in Fig. 16(c)–(e), respectively. The load power and FC delivered power are plotted in Fig. 16(f). Fig. 16(f) shows how K_1 modulates the FC power to attain energy conservation in the ultracapacitor. The estimates $\hat{\eta}_2$ and $\hat{\bar{\eta}}_2$ are shown in Fig. 16(g). The estimates of discharge and charge efficiencies approach $\hat{\eta}_2 \approx 0.85$ and $\hat{\bar{\eta}}_2 \approx 1.05$, respectively. Both efficiency estimates are expected. As mentioned in Section II-C, the charge efficiency $\bar{\eta}_2$ is expected to be greater than 1 since the energy supplied for charging the ultracapacitor will be higher than the change in the stored energy due to losses. It is noted that the learning rate of $\hat{\eta}_2$ and $\hat{\bar{\eta}}_2$ could have potentially been made faster by choosing higher values of the integrator gains. We have deliberately maintained small values for safety of hardware. As mentioned in Section V-A, voltage fluctuations must be small for network safety. Both Figs. 14(b) and 16(b) show small voltage changes ($\leq$0.5 V for $V_{L,\text{nom}} = 24$ or 22 V). Simultaneously, slow rate of efficiency estimation prevents high frequency signals from entering $i_{\text{fc},d}$.

VI. Observations

A. Overall System Loss Trends

While both approaches described above perform satisfactorily in terms of meeting the control objectives, they have certain advantages and disadvantages that make each approach appealing from different perspectives. The voltage-regulation-based approach progressively reduces energy losses; yet it relies on persistent excitation of the load to improve its efficiency estimates. On the other hand, the dissipation-based approach results in uniform energy loss, but it does not require perturbations on the network. The energy losses with each approach were compared and plotted in Fig. 17. Each data point represents an average power loss over an interval, calculated as

$$W_{\text{loss},i} = \frac{1}{t_i - t_{i,0}} \int_{t_{i,0}}^{t_i} (V_L i_L - V_{\text{fc}} i_{\text{fc}})dt \qquad (26)$$

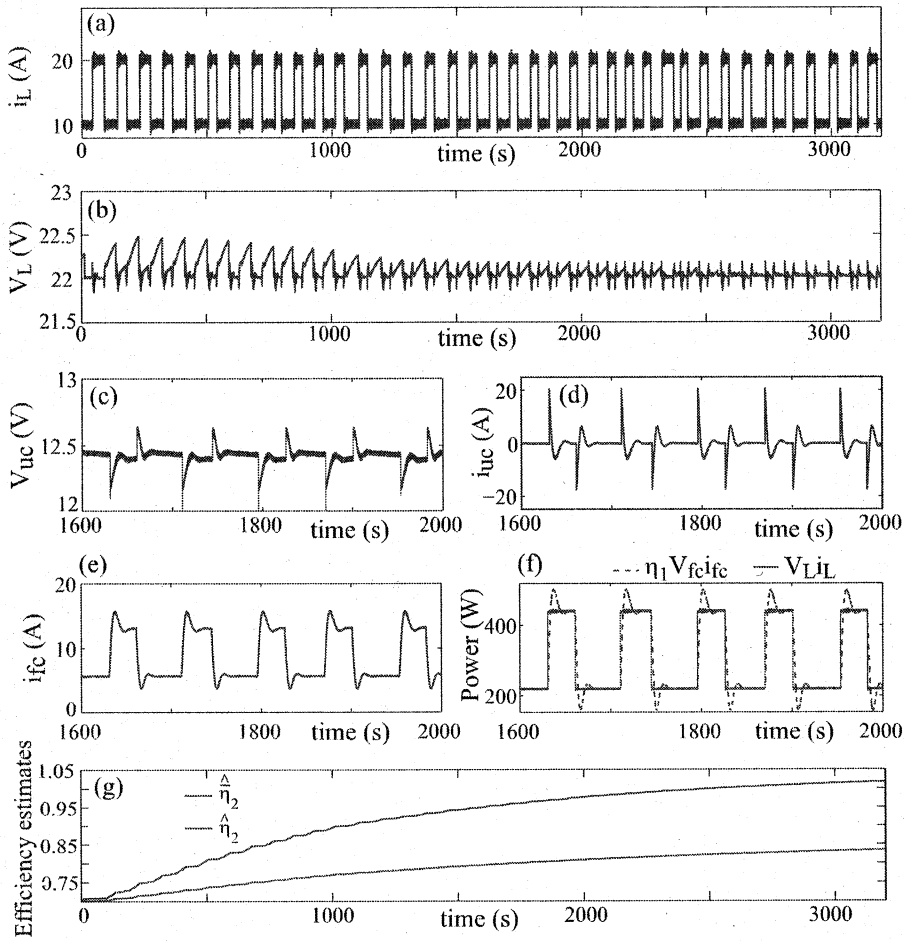

Fig. 16. Experimental results for voltage-regulation-based approach.

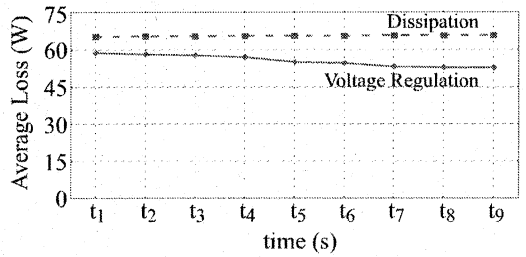

Fig. 17. Power loss trends with voltage regulation and dissipation approaches.

for both approaches. In (26), $\Delta t_i = t_i - t_{i,0}$ represents the ith interval ending at t_i and starting at $t_{i,0}$. Each interval is roughly the same, around 100 s, consisting of one step up and one step down in i_L. The final instants t_i were not all equispaced in time. For example, $(t_5 - t_4)$ and $(t_7 - t_6)$ are longer than the others. It can be observed from the plot that with voltage regulation, the losses decay over time, whereas it is uniform for the dissipation-based approach. The overall magnitudes are not considerably different. This is because the changes in capacitor voltage due to overcharging (and hence the required dissipation) were low in our experiments, owing to a high capacity of 250 F and comparatively lower power levels [see Fig. 13(f)]. It is expected that with lower capacity storage, the advantages of voltage regulation will be more prominent.

B. Fault Tolerance in Decentralized Strategy

As discussed in the Introduction, one advantage of the decentralized approach is fault tolerance. This is illustrated here for the hybrid SOFC system through a simple observation. Referring to prior *centralized control* in [13], the SOFC current demand $i_{fc,d}$ was designed as

$$i_{fc,d} = \frac{V_L i_L}{\bar{\eta}_1 V_{fc}} + g(E_s) + \delta_1(E_s) \tag{27}$$

where $E_s = S - S_t$ and S is the SOC of the ultracapacitor. The function g and the switching parameter δ_1 are both dependent on E_s. However, in the decentralized approach proposed in this paper, $i_{fc,d}$ is designed as given in (12), where the integral E_A is defined in (14). It is clear from (12) and (27) that in the centralized case, the control input $i_{fc,d}$ depends on the SOC, whereas in the latter, the control input is independent of the SOC.

Therefore, even under steady conditions (constant i_L and $S = S_t$), a fault in the ultracapacitor or a fault in sensing

the SOC will deviate the SOFC's delivered power from the steady demanded value of $V_L i_L$. This is because an incorrect value of E_s will result in an incorrect $i_{\mathrm{fc},d}$ in the centralized case, as is clear from (27). This in turn will affect the SOFC's fuel flow rate and cause potential depletion or overcharge and eventual damage of the ultracapacitor. In contrast, in the decentralized controller, the invariance of $i_{\mathrm{fc},d}$ to SOC will ensure $\Delta P = V_L i_L - \eta_1 V_{\mathrm{fc}} i_{\mathrm{fc}} = 0$ even under such a fault. This is implied from the result of Theorem 1. The effectiveness of decentralized over centralized control is also dependent on the nature of faults. For certain faults, such as the one mentioned here, the advantage may be clear, but for others, secondary protection logic may be necessary for both approaches.

VII. Conclusion

Distributed control for power management in a hybrid FC ultracapacitor system is demonstrated through simulations and experiments. In the proposed decentralized framework, individual controllers for the FC and the ultracapacitors use local information only. The system as a whole guarantees load-following in the presence of rapidly fluctuating power demands without jeopardizing any component. It is shown that simple decentralized controllers can be built by locally applying conservation of energy. Moreover, robust performance can be achieved through controlled dissipation of excess energy or by voltage modulation. The latter effectively amounts to establishing implicit communication between the controllers using the power line itself. Stability analysis is carried to ascertain the efficacy of the individual controllers. Elements of fault tolerance are shown to be inherent in the decentralized approach. Extending this approach to broader networks with many power sources and storage elements is an area of ongoing and future research. Here, the challenges expected are in autotuning of steady-state power among distributed resources, while maintaining stability. Another question of importance will be the management of multiple energy storage elements. Overall, an integration of feedback control and optimization problems will evidently be required.

References

[1] J. Larminie and A. Dicks, *Fuel Cell Systems Explained*, 2nd ed. New York, NY, USA: Wiley, 2003.

[2] X. Li, *Principles Fuel Cells*. New York, NY, USA: Taylor & Francis, 2006.

[3] M. H. Nehrir and C. Wang, *Modeling and Control of Fuel Cells: Distributed Generation Applications*. New York, NY, USA: Wiley, 2009.

[4] J. R. Meacham, F. Jabbari, J. Brouwer, J. L. Mauzey, and G. S. Samuelsen, "Analysis of stationary fuel cell dynamic ramping capabilities and ultra capacitor energy storage using high resolution demand data," *J. Power Sour.*, vol. 156, no. 2, pp. 472–479, 2006.

[5] T. Das and S. Snyder, "Adaptive control of a solid oxide fuel cell ultracapacitor hybrid system," *IEEE Trans. Control Syst. Technol.*, vol. 21, no. 2, pp. 372–383, Mar. 2013.

[6] R. Gaynor, F. Mueller, F. Jabbari, and J. Brouwer, "On control concepts to prevent fuel starvation in solid oxide fuel cells," *J. Power Sour.*, vol. 180, no. 1, pp. 330–342, 2008.

[7] F. Mueller, F. Jabbari, and J. Brouwer, "On the intrinsic transient capability and limitations of solid oxide fuel cell systems," *J. Power Sour.*, vol. 187, no. 2, pp. 452–460, 2009. [Online]. Available: http://www.sciencedirect.com/science/article/pii/S0378775308021575

[8] F. Mueller, F. Jabbari, R. Gaynor, and J. Brouwer, "Novel solid oxide fuel cell system controller for rapid load following," *J. Power Sour.*, vol. 172, no. 1, pp. 308–323, 2007. [Online]. Available: http://www.sciencedirect.com/science/article/pii/S0378775307011408

[9] S. Campanari, "Thermodynamic model and parametric analysis of a tubular SOFC module," *J. Power Sour.*, vol. 92, nos. 1–2, pp. 26–34, 2001. [Online]. Available: http://www.sciencedirect.com/science/article/pii/S0378775300004948

[10] A. Lazzaretto, A. Toffolo, and F. Zanon, "Parameter setting for a tubular SOFC simulation model," *J. Energy Resour. Technol.*, vol. 126, no. 1, pp. 40–46, May 2004.

[11] M. Nayeripour, M. Hoseintabar, and T. Niknam, "A new method for dynamic performance improvement of a hybrid power system by coordination of converter's controller," *J. Power Sour.*, vol. 196, no. 8, pp. 4033–4043, 2011. [Online]. Available: http://www.sciencedirect.com/science/article/pii/S0378775310021488

[12] T. Das, S. Narayanan, and R. Mukherjee, "Steady-state and transient analysis of a steam-reformer based solid oxide fuel cell system," *J. Fuel Cell Sci. Technol.*, vol. 7, no. 1, p. 011022, 2010.

[13] T. Allag and T. Das, "Robust control of solid oxide fuel cell ultracapacitor hybrid system," *IEEE Trans. Control Syst. Technol.*, vol. 20, no. 1, pp. 1–10, Jan. 2012.

[14] Y. Guezennec, T.-Y. Choi, G. Paganelli, and G. Rizzoni, "Supervisory control of fuel cell vehicles and its link to overall system efficiency and low-level control requirements," in *Proc. Amer. Control Conf.*, 2003, pp. 2055–2061.

[15] M. Grujicic, K. M. Chittajallu, and J. T. Pukrushpan, "Control of the transient behaviour of polymer electrolyte membrane fuel cell systems," *Proc. Inst. Mech. Eng. D, J. Automobile Eng.*, vol. 218, no. 11, pp. 1239–1250, 2004.

[16] J. Sun and I. V. Kolmanovsky, "Load governor for fuel cell oxygen starvation protection: A robust nonlinear reference governor approach," *IEEE Trans. Control Syst. Technol.*, vol. 13, no. 6, pp. 911–920, Nov. 2005.

[17] C. H. Woo and J. B. Benziger, "PEM fuel cell current regulation by fuel feed control," *Chem. Eng. Sci.*, vol. 62, no. 4, pp. 957–968, 2007.

[18] A. Vahidi, A. Stefanopoulou, and H. Peng, "Current management in a hybrid fuel cell power system: A model-predictive control approach," *IEEE Trans. Control Syst. Technol.*, vol. 14, no. 6, pp. 1047–1057, Nov. 2006.

[19] A. E. Auld, K. M. Smedley, F. Mueller, J. Brouwer, and G. S. Samuelsen, "Load-following active power filter for a solid oxide fuel cell supported load," *J. Power Sour.*, vol. 195, no. 7, pp. 1905–1913, 2010. [Online]. Available: http://www.sciencedirect.com/science/article/pii/S037877530901739X

[20] P. Thounthong, S. Pierfederici, J.-P. Martin, M. Hinaje, and B. Davat, "Modeling and control of fuel cell/supercapacitor hybrid source based on differential flatness control," *IEEE Trans. Veh. Technol.*, vol. 59, no. 6, pp. 2700–2710, Jul. 2010.

[21] P. Adhikari and M. Abdelrahman, "Modeling, control, and integration of a portable solid oxide fuel cell system," *J. Fuel Cell Sci. Technol.*, vol. 9, no. 1, p. 011010, 2012.

[22] A. Vahidi and W. Greenwell, "A decentralized model predictive control approach to power management of a fuel cell-ultracapacitor hybrid," in *Proc. Amer. Control Conf.*, Jul. 2007, pp. 5431–5437.

[23] A. Y. Sendjaja and V. Kariwala, "Decentralized control of solid oxide fuel cells," *IEEE Trans. Ind. Informat.*, vol. 7, no. 2, pp. 163–170, May 2011.

[24] L. Bakule, "Decentralized control: An overview," *Annu. Rev. Control*, vol. 32, no. 1, pp. 87–98, 2008. [Online]. Available: http://www.sciencedirect.com/science/article/pii/S1367578808000096

[25] W. M. Haddad, Q. Hui, V. Chellaboina, and S. G. Nersesov, "Hybrid decentralized maximum entropy control for large-scale dynamical systems," *Nonlinear Anal., Hybrid Syst.*, vol. 1, no. 2, pp. 244–263, 2006.

[26] A. Ramakrishna and N. Viswanadham, "Decentralized control of interconnected dynamical systems," in *Proc. 19th IEEE Conf. Decision Control Including Symp. Adapt. Process.*, Dec. 1980, pp. 538–543.

[27] Y. Guo, D. J. Hill, and Y. Wang, "Nonlinear decentralized control of large-scale power systems," *Automatica*, vol. 36, no. 9, pp. 1275–1289, 2000.

[28] V. A. Ugrinovskii and H. R. Pota, "Decentralized control of power systems via robust control of uncertain Markov jump parameter systems," in *Proc. 43rd IEEE Conf. Decision Control*, Dec. 2004, pp. 3503–3508.

[29] A. A. Aquino-Lugo, "Distributed and decentralized control of the power grid," Ph.D. dissertation, Dept. Elect. Comput. Eng., Univ. Illinois Urbana–Champaign, Champaign, IL, USA, 2011.

[30] A. Tuladhar, K. Jin, T. Unger, and K. Mauch, "Parallel operation of single phase inverter modules with no control interconnections," in *Proc. 12th Annu. Appl. Power Electron. Conf. Expo. (APEC)*, vol. 1. Feb. 1997, pp. 94–100.

[31] P. Hines and S. Talukdar, "Reciprocally altruistic agents for the mitigation of cascading failures in electrical power networks," in *Proc. 1st Int. Conf. Infrastruct. Syst. Services, Building Netw. Brighter Future (INFRA)*, Nov. 2008, pp. 1–6.

[32] D. Chiappini, A. L. Facci, L. Tribioli, and S. Ubertini, "SOFC management in distributed energy systems," *J. Fuel Cell Sci. Technol.*, vol. 8, no. 3, p. 031015, 2011.

[33] A. K. Saha, S. Chowdhury, S. P. Chowdhury, and Y. H. Song, "Application of solid-oxide fuel cell in distributed power generation," *IET Renew. Power Generat.*, vol. 1, no. 4, pp. 193–202, 2007.

[34] A. Sakhare, A. Davari, and A. Feliachi, "Fuzzy logic control of fuel cell for stand-alone and grid connection," *J. Power Sour.*, vol. 135, nos. 1–2, pp. 165–176, 2004. [Online]. Available: http://www.sciencedirect.com/science/article/pii/S0378775304005385

[35] F. Mueller, J. Brouwer, F. Jabbari, and S. Samuelsen, "Dynamic simulation of an integrated solid oxide fuel cell system including current-based fuel flow control," *J. Fuel Cell Sci. Technol.*, vol. 3, no. 2, pp. 144–154, 2006.

[36] R. Kandepu, L. Imsland, B. A. Foss, C. Stiller, B. Thorud, and O. Bolland, "Modeling and control of a SOFC-GT-based autonomous power system," *Energy*, vol. 32, no. 4, pp. 406–417, Apr. 2007.

[37] T. Das and R. Weisman, "A feedback based load shaping strategy for fuel utilization control in SOFC systems," in *Proc. Amer. Control Conf. (ACC)*, 2009, pp. 2767–2772.

[38] V. Tsourapas, A. G. Stefanopoulou, and J. Sun, "Model-based control of an integrated fuel cell and fuel processor with exhaust heat recirculation," *IEEE Trans. Control Syst. Technol.*, vol. 15, no. 2, pp. 233–245, Mar. 2007.

[39] A. Drolia, P. Jose, and N. Mohan, "An approach to connect ultracapacitor to fuel cell powered electric vehicle and emulating fuel cell electrical characteristics using switched mode converter," in *Proc. 29th Annu. Conf. IEEE Ind. Electron. Soc. (IECON)*, Nov. 2003, pp. 897–901.

[40] A. Arce, A. J. del Real, and C. Bordons, "MPC for battery/fuel cell hybrid vehicles including fuel cell dynamics and battery performance improvement," *J. Process Control*, vol. 19, no. 8, pp. 1289–1304, 2009. [Online]. Available: http://www.sciencedirect.com/science/article/pii/S0959152409000420

[41] W. Greenwell and A. Vahidi, "Predictive control of voltage and current in a fuel cell–ultracapacitor hybrid," *IEEE Trans. Ind. Electron.*, vol. 57, no. 6, pp. 1954–1963, Jun. 2010.

[42] A. G. Stefanopoulou and K.-W. Suh, "Mechatronics in fuel cell systems," *Control Eng. Pract.*, vol. 15, no. 3, pp. 277–289, 2007.

[43] H. K. Khalil, *Nonlinear Systems*, 3rd ed. Upper Saddle River, NJ, USA: Prentice-Hall, 2002.

[44] W. J. Rugh, *Linear System Theory*, 2nd ed. Upper Saddle River, NJ, USA: Prentice-Hall, 1996.

[45] G. F. Franklin, J. Da Powell, and A. Emami-Naeini, *Feedback Control of Dynamic Systems*, 6th ed. Upper Saddle River, NJ, USA: Prentice-Hall, 2009.

[46] *Single 9-A High-Speed Low-Side MOSFET Driver With Enable*. [Online]. Available: http://www.ti.com/lit/ds/slusa13b/slusa13b.pdf, accessed Sep. 9, 2014.

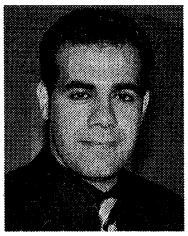

Omid Madani received the B.S. degree in mechanical engineering from the Sharif University of Technology, Tehran, Iran, in 2009, and the M.S. and Ph.D. degrees from the University of Central Florida, Orlando, FL, USA, in 2011 and 2014, respectively.

His Ph.D. research was focused on decentralized power management of fuel cells and developing control strategies for energy systems using multivariable design approach. Since 2014, he has been with CD-adapco Inc., Orlando, as a Senior Engineer.

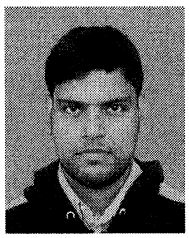

Amit Bhattacharjee received the B.E. degree in electrical engineering from Jadavpur University, Kolkata, India, in 2008, and the M.S. degree from the University of Central Florida (UCF), Orlando, FL, USA, in 2014, where he is currently pursuing the Ph.D. degree.

His M.S. thesis research was involved in the area of decentralized power management of microgrids with UCF. He worked in the power distribution industry and was involved in power electronics research for more than three years.

Tuhin Das (M'09) received the B.Tech. degree from IIT Kharagpur, Kharagpur, India, in 1997, and the M.S. and Ph.D. degrees from Michigan State University, East Lansing, MI, USA, in 2000 and 2002, respectively, all in mechanical engineering.

He has been with the industry for four years and was a Faculty Member of mechanical engineering with the Rochester Institute of Technology, Rochester, NY, USA. His research has been funded by NSF, ONR, and Siemens. He is currently an Assistant Professor of Mechanical and Aerospace Engineering with the University of Central Florida, Orlando, FL, USA. His current research interests include mobile robots, fuel cells, and wind energy.